Diagnosis and prognosis of neuroendocrine tumours of the lung by means of high resolution image analysis

Uta Jütting [a,*], Peter Gais [b], Karsten Rodenacker [a], Joachim Böhm [c], Susanne Koch [b], Heinz W. Präuer [d] and Heinz Höfler [b,c]

[a] *Institute for Biomathematics and Biometry, GSF-National Research Center for Environment and Health, Neuherberg, Germany*
[b] *Institute of Pathology, GSF-National Research Center for Environment and Health, Neuherberg, Germany*
[c] *Institute of Pathology, Technical University of Munich, School of Medicine, Munich, Germany*
[d] *Department of Surgery, Technical University of Munich, School of Medicine, Munich, Germany*

Received 6 July 1998
Revised 28 January 1999
Accepted 27 March 1999

Neuroendocrine tumours (NET) of the lung are divided in subtypes with different malignant potential. The first is the benign or low-grade malignant tumours, well-differentiated, called typical carcinoids (TC) and the second is the high-grade malignant tumours, poorly differentiated of small (SCLC) or large cell type (LCLC). Between these tumour types lies the well-differentiated carcinoma with a lower grade of malignancy (WDNEC). In clinical routine it is very important with regard to prognosis to distinguish patients with low malignant potential from those with higher ones. In this study 32 cases of SCLC, 13 of WDNEC and 14 of TC with a follow-up time up to 7 years were collected. Sections 4 μm thick from paraffin embedded tissue were Feulgen stained. By means of high resolution image analysis 100 nuclei per case were randomly gathered to extract morphometric, densitometric and textural quantitative features. To investigate the ploidy status of the tumour the corrected DNA distribution was calculated. Stepwise linear discriminant analysis to differentiate the classes and Cox regression analysis for the survival time analysis were applied. Using chromatin textural and morphometric features in two two-class discriminations, 11 of the 14 TC cases and 8 of the 13 WDNEC cases were correctly classified and 11/13 WDNEC cases and 28/32 SCLC cases, respectively. The WDNEC cases are more similar in chromatin structure to TC than to SCLC. For the survival analysis, only chromatin features were selected to differentiate patients with better and worse prognosis independent of staging and tumour type.

Keywords: Neuroendocrine lung tumours, carcinoid, small cell carcinoma, textural features, image analysis, DNA distribution, prognosis

1. Introduction

In industrial countries lung cancer is the most frequent cause of death for men and women. The overall 5-year survival rate is now 15%. The most important risk factor is smoking, followed by chemically noxious substances (asbestos, arsenic, uranium, etc.) and genetic factors [34].

The malignant potential of neuroendocrine tumours varies considerably. Benign or low by grade malignant, well-differentiated tumours, called typical carcinoids (TC) or well differentiated neuroendocrine tumours (WDNET) [7,19] low-grade malignant, well-differentiated carcinoma (WDNEC) or 'atypical carcinoids' and high grade malignant, poorly differentiated carcinoma from large or small cell type (SCLC) are histologically clearly defined [10,15,27,28,34,38, 39,41]. The treatment schemes for the different tumour types are the complete resection of the tumour in case of TC and WDNEC, followed, in some cases, by an adjuvant chemo- or radiotherapy. For SCLC different therapy schemes are applied: surgery, chemo- and radiotherapy in combinations. Patients with typical carcinoid tumours have an excellent prognosis (lethal

*Address for correspondence: Uta Jütting, GSF-Institute for Biomathematics and Biometry, Ingolstädter Landstr. 1, D-85764 Oberschleißheim, Germany. Tel.: +49 89 3187 2555; Fax.: +49 89 3187 3127; E-mail: uta.juetting@gsf.de.

Analytical Cellular Pathology 18 (1999) 109–119
ISSN 0921-8912 / $8.00

rate 5–15% within 5 years), whereas patients suffering SCLC have only a poor prognosis [4,9,33,38]. In general the histopathological distinction of both these tumour types should not cause difficulties for pathologists. However, for patients with a WDNEC their individual prognosis is difficult to predict. Recognized prognosis factors until now are the staging and histological type. Additional independent factors for different subtypes of carcinomas could be grading, oncogenes (K-ras, c-Myc, n-Myc), CEA, MIB 1, AgNOR, p53, c-erB-2 and ploidy. Examples of studies in these fields are given in [4,5,8,9,11,20,22–24,29,30,33,37]. However the results are not yet always convincing. They have to be validated in further studies. Investigations by means of high resolution image analysis from sections using chromatin features are not yet published.

2. Material and methods

Formalin-fixed and paraffin-embedded sections of 32 cases of SCLC, 13 cases of WDNEC and 14 cases of TC were collected from clinical routine. Resection material was obtained from all operated patients and endoscopic biopsies were available from some SCLC cases. The 4 μm thick sections were stained according to our Feulgen procedure. In brief: The slides were fixed in 70% ethanol for 15 min. and subsequently stained (hydrolysis: 5 N HCl, 22°C, 30 min; Schiff reagent: 1 h) [1].

2.1. Clinical data

For most of the patients the complete clinical data: tumour stage at time of diagnosis, therapeutic strategy, age, sex and the follow up time were available. In Table 1 these data are listed separately for each tumour class. Patients who died of surgical complications within one month were excluded from this study. All patients with TC were only underwent surgery, whereas the others had an adjuvant therapy (chemo- or/and radiotherapy) as well. All SCLC cases were also classified in an oat-cell type (cytoplasm only present marginally) or in an intermediate-cell type (cytoplasm more prominent, larger polygonal cells). There is no known validated difference between these histological subtypes in terms of prognosis.

2.2. Data acquisition

About 100 single tumour cell nuclei and 20 leukocytes (for DNA standardization) per slide were randomly selected in the tumour area with an Axiomat-microscope (Zeiss, Oberkochen, Germany), equipped with a TV-camera (Bosch, T1VK9B1, Stuttgart, Germany, 128 $\times$ 128 pixels). The cells were scanned in transmission with a 100$\times$ objective (oil immersion, numerical aperture 1.3) using an optical narrow band filter of 548 nm wavelength. The pixel distance was 0.25 μm, and the nominal grey value resolution was covered by 256 channels [12]. Processing of digitized images was carried out using a VAX 4000-500 processor (Digital, Maynard, USA) with software written in idl (Interactive Data Language, RSI, Boulder, CO, USA). Each nuclei was focused individually at its border to maintain reproducibility. A shading correction was performed to eliminate systematical errors related to the light or optical conditions. For feature extraction nuclei were segmented automatically under visual control and interactive improvement when necessary. Morphological, densitometrical and textural features were calculated using the extinction or optical density image which was derived from transmission image [31]. Features like mean, standard deviation, coefficient of variation and range were calculated from the histogram of the measured nucleus as well as from bright and dark particle regions inside the object which were automatically segmented [13,31]. For the latter a grey scale skeleton was applied on the extinction image (upper skeleton) and on its inversion (lower skeleton), which delivers the partitions into regions around dark and bright particles. The skeleton is calculated by a watershed algorithm. For chromatin distribution features, several transformations were obtained by using linear and non-linear filtering such as Roberts gradient, Laplace transform and the flat texture image (difference between extinction image and median filtered one), local fractal and multi-fractal dimensions, topographical gradient, the difference of upper and lower skeleton (a topographical gradient), and statistical features from runlength and co-occurrence matrix [26,32, 40,42]. These textural features are derived from pattern recognition methods.

For classification only those features were offered which were shown to be nearly independent of staining intensity and of the specimens thickness [16,32]. The remaining feature set contained about 60 variables. A total of 3513 tumour nuclei of SCLC, 1482 of WDNEC and 1632 of TC were measured.

Table 1
Clinical data of 59 tumour patients of the lung separately for each tumour type

32 SCLC:	
Sex	4 female, 28 male
Age	MV = 59.7 years, range (38 to 77 years)
Cell type	16 OAT, 16 ITM
Tumour size	5 T1, 19 T2, 7 T3, 1 Tx
Lymph node involvement	8 N0, 8 N1, 11 N2, 2 N3, 3 Nx
Metastasis	21 M0, 10 M+, 1 Mx
Stage	10 EXT, 22 LIM
Therapy	OP and/or R and/or CH
Survival time	MV = 21.2 months, range (2 to 89 months)
	26 patients deceased
13 WDNEC:	
Sex	7 female, 6 male
Age	MV = 51.5 years, range (19 to 71 years)
Tumour size	MV = 3.2 cm, range (0.9 to 9 cm)
Lymph node involvement	7 N0, 6 N+
Therapy	OP and/or R and/or CH
Survival time	MV = 30.9 months, range (4 to 61 months)
	3 patients deceased
14 TC:	
Sex	6 female, 8 male
Age	MV = 53.6 years, range (22 to 67 years)
Tumour size	MV = 2.8 cm, range (1.2 to 6 cm)
Lymph node involvement	10 N0, 4 N+
Therapy	OP
Survival time	MV = 44.9 months, range (12 to 92 months)
	1 patient deceased

LIM = limited disease, EXT = extensive disease, OP = operation, CH = chemotherapy, R = radiotherapy, OAT = oat cell type, ITM = intermediate cell type.

The features used are briefly described in the Appendix.

For investigation of the relevance of features for prognosis, the mean value, median and the CV of each feature per specimen were calculated. For those MV, MED or CV is given in parenthesis.

2.3. DNA-features

Although all specimens have been cut in to 4 μm slices their true thickness was measured by a laser scanning microscope at five locations per specimen. The mean thickness for all specimens was 6.3 μm ($\pm 1.9\,\mu$m, range: 2.5–11 μm). For each tumour cell and leukocyte, the area and the mean optical density were calculated and from these the integrated optical density was calculated. Due to the slicing problem of nuclei in histological sections, the integrated optical density was corrected by the thickness of the specimen. The formulae are given in Haroske et al. [17,18]. To normalize the IOD-histogram in c-values the lymphocyte peak of IOD was set to 80% of 2c, due to the underestimation (non-stoichiometric Feulgen reaction of dark/pynotic nuclei) of the lymphocytes in sections [1]. The tumour cells were normalized according to this factor. The normalization procedure is correct for round objects. Nevertheless this was performed for all nuclei for the DNA distributions for stemline ploidy and proliferation. In Fig. 1 some typical DNA distributions are shown for the three classes. From the DNA distribution the mean value, 5c-exceeding rate, entropy and 2c-deviation index were calculated to test the correlation of the three classes and of prognosis [2,3,14, 35,36]. These features are only slightly influenced by small standardization errors.

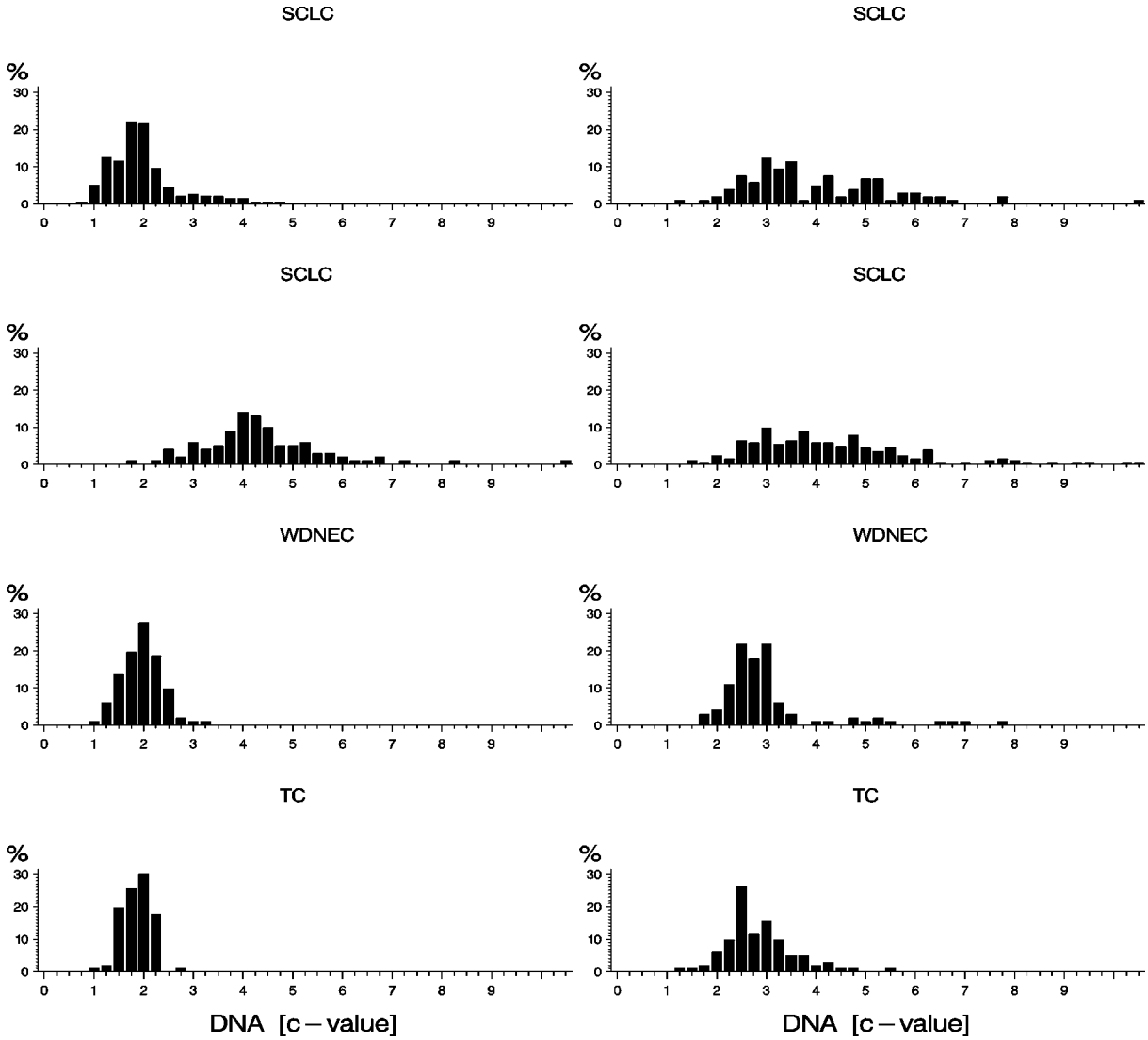

Fig. 1. Examples of typical DNA-distributions for the 3 different classes SCLC, WDNEC and TC.

3. Statistics

3.1. Discrimination on the cell level

The statistical evaluations were done using SAS (SAS Institute, Inc., Cary, NC, USA) and BMDP (Statistical Software Inc., Los Angeles, CA, USA) program packages. All nuclei from specimens of the same clinical samples were pooled and the classifier was designed in two-class stepwise linear discriminate analyses. Out of the evaluated feature set only those features were used in the classification steps which are univariately significant. Up to 10 features were stepwise selected either accepted for the succeeding hold-one-out classification or the procedure was stopped due to a non-significant F-value. The value for the first selected feature is the univariate one whereas the following F-values are multivariate reflecting the impact of results after using this feature together with the already selected features. For each specimen, the mean of the a posteriori probability (APOP) distribution of the corresponding cells was calculated. For the specimen classification, this APOP value and the double standard error of the mean (SEM) were used. A specimen was classified into that class with the highest APOP value only if the mean APOP $\pm$ SEM did not cut a threshold (THR) which was set as the border between the two classes (APOP $=$ 0.5). Cases with THR$\in$\{APOP $\pm$ 2SEM\}

were considered as unclear [6]. The significance for the specimen classifications was calculated using contingency tables without defining unclear cases.

3.2. Prognosis

For all discrete features the Kaplan–Meier curves were plotted to find the best strata for the Cox regression analysis which is sensitive for decrease or increase of feature values with survival time [21]. Different defined classes with comparable survival curves were pooled by visual inspection. Then after optimizing the strata all features were tested by means of the Cox regression analysis [25], first univariate then multivariate. To demonstrate the importance of a multivariate analysis, Kaplan–Meier curves for different strata and individual survival curves for patients were plotted.

All statistical evaluations were considered to be significant at the 95% level.

4. Results

4.1. DNA-ploidy

The DNA-distributions were classified into three classes: stemline near-diploid non-proliferating (limited to cells outside 2c-peak), stemline near-diploid proliferating and clear aneuploid distribution (Table 2) [14]. A higher percentage of aneuploid DNA distributions are found in the SCLC cases than in both the other tumour types. However a clear association cannot be seen, in all three classes in which diploid and aneuploid distributions are present. The DNA parameter entropy, 5c-exceeding rate, mean value and 2c-deviation index are only significant for the discrimination of SCLC with TC and WDNEC, respectively (Table 3).

Table 2
Proliferation of the tumours

	Near diploid non-proliferating	Near diploid proliferating	Aneuploid	Total
TC	12	–	2	14
WDNEC	11	–	2	13
SCLC	12	10	10	32

Table 3
DNA-parameters: mean values and significance

	TC	WDNEC	SCLC
DNA mean value	2.05	2.05	2.77
5c-exceeding rate	0.4%	1.2%	6.6%
Entropy	3.8	3.8	4.7
2c-dev. index	0.36	0.57	0.91

Significance for	TC-WDNEC	TC-SCLC	WDNEC-SCLC
DNA mean value	n.s.	$p < 0.01$	$p < 0.01$
5c-exceeding rate	n.s.	$p < 0.01$	$p < 0.05$
Entropy	n.s.	$p < 0.001$	$p < 0.001$
2c-dev. index	n.s.	$p < 0.01$	n.s.

4.2. Discrimination of SCLC and WDNEC

The cells of SCLC and WDNEC were pooled, and the stepwise linear discriminant analysis was applied. The most discriminating features were HUCV, P and M3, which demonstrates the importance of chromatin texture and shape of the nuclei. HUCV reflects a more balanced distribution of heterochromatin, segmented by means of their topographical arrangement by watershed (for feature description see appendix). In Fig. 2 6 nuclei with low (≅0.10 [A.U.]) values of HUCV (representing nuclei of SCLC) and 6 with high (≅0.27 [A.U.]) values of HUCV (representing nuclei of WDNEC) are shown. The overall correct classification rate was 75.2%, 73.9% for SCLC and 76.5% for WDNEC. The subsequent specimen classification led to 11/13 correct classification (84.6%) for WDNEC and 25/32 (78.1%) for SCLC, respectively. Seven cases remained unclear. Without unclear decisions two WDNEC cases and four SCLC case were incorrectly classified (Table 4). The significance of the result was $p < 0.0001$. For demonstration of the specimen classification results the APOP value of each specimen ranked according to its value is given in Fig. 3.

4.3. Discrimination of TC and WDNEC

The cell classification rate was for the TC 63.6% and 65.3% for WDNEC. 9/14 TC patients (64.3%) and 8/13 WDNEC patients (61.5%) were correctly classified. Four cases were incorrectly classified, the rest was unclear. Without defining the unclear class three TC cases and five WDNEC cases remained in the other class. The result is significant for $p < 0.05$. The most important features were DCV (variation of density of dark particles), P and CO14, which again demonstrates the importance of chromatin and shape (Table 5).

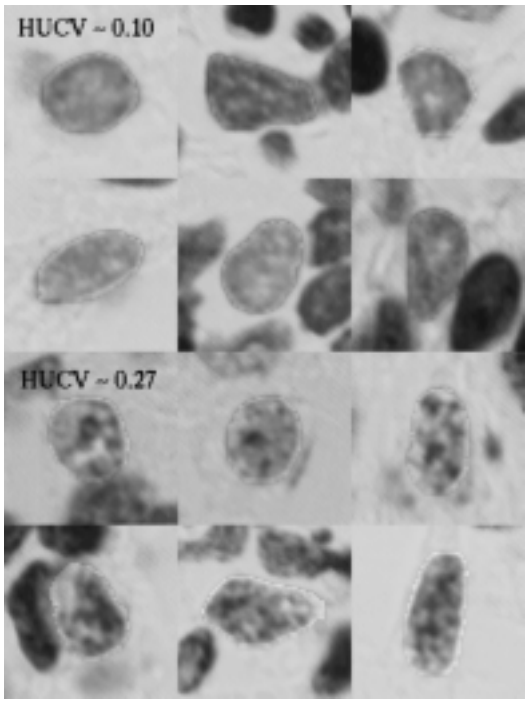

Fig. 2. Six nuclei (two upper rows) with low (0.11 [A.U.]) and six nuclei (two lower rows) with high (0.27 [A.U.]) values of HUCV.

Table 4
Specimen classification results of WDNEC and SCLC and selected features with F-values

Specimen classification

	WDNEC	SCLC	Unclear	Total	% Correct
WDNEC	11	1	1	13	84.6
SCLC	1	25	6	32	78.1
					80.0

Specimen classification

	WDNEC	SCLC	Total	% Correct
WDNEC	11	2	13	84.6
SCLC	4	28	32	87.5
				86.7

$p < 0.0001$. Selected features and F-values: HUCV (396.4), P (648.9), M3 (229.7), NC1 (91.9), RL1 (62.3).

4.4. *Discrimination of TC and SCLC with testset WDNEC*

To investigate whether nuclei of WDNEC cases are more similar in the chromatin structure and/or shape to TC or SCLC, the discrimination was calculated using TC and SCLC nuclei only. In this case HUCV, P and RL4 were the most important features. The overall correct classification rate was 81.8%. Using the class

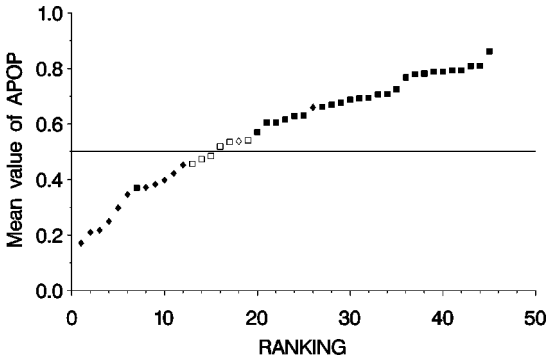

Fig. 3. Specimen classification results of WDNEC and SCLC (■ SCLC cases, ♦ WDNEC cases, open symbols: unclear decisions).

Table 5
Specimen classification results of TC and WDNEC and selected features with F-values

Specimen classification

	TC	WDNEC	Unclear	Total	% Correct
TC	9	2	3	14	64.3
WDNEC	3	8	2	13	61.5
					63.0

Specimen classification

	TC	WDNEC	Total	% Correct
TC	11	3	14	78.6
WDNEC	5	8	13	61.5
				70.3

$p < 0.05$. Selected features and F-values: DVC (121.8), P (83.2), CO14 (33.2), BICV (46.8), MM3 (22.1).

WDNEC as a testset, 927 nuclei (62.6%) were classified into TC and 555 into SCLC. The specimen classification step led to three cases classified as SCLC and eight cases as TC, the remaining two remained unclear. Without unclear decisions these two cases were classified as TC. This result demonstrates that most cases of the WDNEC in our study have a chromatin structure more similar to TC. The results are given in Table 6 and Fig. 4.

4.5. *Discrimination of oat-cell type carcinomas (OAT) and intermediate-cell type (ITM) in case of SCLC*

All cases of SCLC were additionally classified in types of intermediate or oat cells. By means of the chromatin features HUNO, HUEULER and RFM1 an overall cell classification rate of 67.5% could be achieved. 11/16 cases of ITM and 12/16 cases of OAT were correctly classified ($p < 0.05$).

Table 6
Specimen classification results of TC and SCLC using WDNEC as a test set and selected features with F-values

Specimen classification

	TC	SCLC	Unclear	Total	% Correct
TC	12	1	1	14	64.3
SCLC	1	28	3	32	87.5
WDNEC	8	3	2	13	

Specimen classification

	TC	SCLC	Total	% Correct
TC	13	1	14	92.9
SCLC	3	29	32	90.6
WDNEC	10	3	13	

$p < 0.0001$. Selected features and F-values: HUCV (863.5), P (1500.4), RL4 (136.2), HUSPAN (86.6), FO1 (78.2).

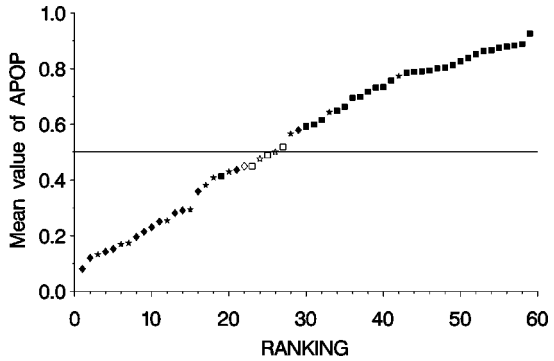

Fig. 4. Specimen classification results of TC and SCLC using WDNEC as a test set (♦ TC cases, ■ SCLC cases, ⋆ WDNEC cases, open symbols: unclear decisions).

4.6. Survival analysis

Stepwise Cox regression analysis was applied to search for the features that correlated best with survival time. Only those features that were univariately significant are given have. The DNA parameters are correlated at $p < 0.001$. The clinical parameters such as histological type, pT, pN and pM are, as expected, highly significant, but sex and age of the patients are not. However, the clinical data were not included in the survival analysis and neither cases were with unknown patient's data, e.g., if the material was collected before surgery.

Five chromatin features were selected in case of survival analysis which led to the Cox variable:

$$\mathrm{COX} = 0.04 \times \mathrm{IM2(CV)} + 0.58 \times \mathrm{NR3(CV)} + 4.69 \times \mathrm{CO10(MED)} - 128 \times \mathrm{CO11(MED)} + 10.44 \times \mathrm{DNOA(MED)} + 250.$$

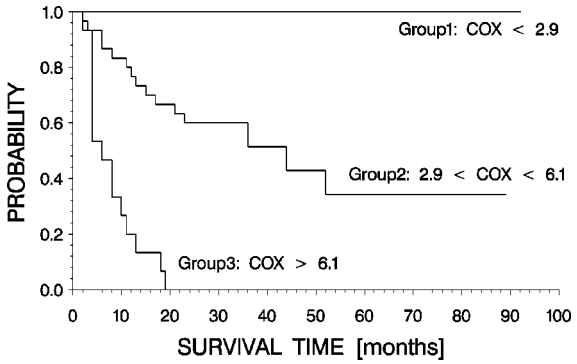

Fig. 5. Kaplan–Meier survival curves for three patient groups according to the Cox regression analysis.

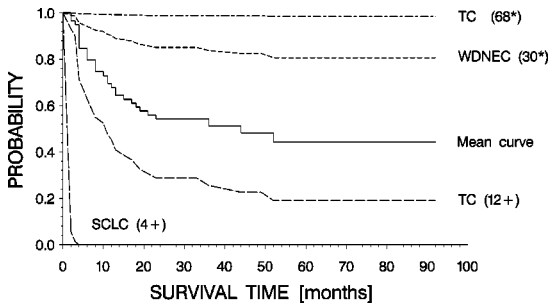

Fig. 6. Individual survival curves for four patients according to the Cox regression analysis and mean survival curve for all patients (⋆ patient still alive, + patient died).

To demonstrate the efficiency of the results, three Kaplan–Meier survival curves were plotted (Fig. 5). In the first strata 15 patients with the lowest values of the Cox variables are pooled, in the third strata those of 14 patients with the highest values. The remaining cases are in the second curve. The Wilcoxon test led to a significance of $p < 0.0001$. In the strata with the worst prognosis all 14 patients died within 20 months. In Fig. 6 individual survival curves for four patients were plotted together with the mean survival curve.

5. Discussion

In the last decades high resolution image cytometry and histometry has become an established tool in the investigation of different problems in clinical routine. Most efforts were dedicated originally to the cervical field, followed by breast carcinoma, bladder and other

tumour types from different sites. In this study we used neuroendocrine lung tumours to demonstrate that textural and morphometric features, evaluated by means of high resolution image histometry, are useful to distinguish nuclei from different tumour types as well as to correlate them with the survival time of the patients.

Most of the publications using parameters derived from DNA distributions were done by means of flow cytometry. The shortcomings of this method are well known, e.g., the measurement of doublets and artefacts. However, in histometry the accuracy of DNA-distributions is also questionable due to the cutting problems of the cell nuclei with different shapes. Stereology-based algorithms were developed to recalculate the real distributions but they are not well applicable in all cases [17]. In our study, two of the 14 TC have a clear aneuploid DNA distribution whereas the others are near diploid with 5c-exeeding rates under 2%. This is in accordance with the investigations given in the summary in [34] with 80% euploid tumours. The percentage of euploid tumour types for WDNEC is much higher (11/14) than one can find in the literature (≈20%). The 5c-exceeding rates are below 2% except in two cases with 6%. The DNA-distributions of the SCLC differ from non-proliferating euploid types to high-proliferating aneuploid ones. The calculated DNA-parameters are significant for the discrimination of SCLC from both of the other classes, but however are not significant for TC and WDNEC.

In some publications using flow cytometry, significant results were found using ploidy index and proliferation activity as predictor for aggressive behaviour in lung carcinomas [8,9,11,29,37]. However, the results are difficult to compare due to the different selection of lung cancer types [27]. Some of the authors concentrated on the non-small cell lung carcinomas, others investigated only cases with comparable stage or small cell carcinomas.

Only in some studies was the relevance of immunocytochemical staining already investigated in different lung cancer specimens. Significant results were found in cases of non-small cell cancer. MIB 1, Ki-67, bcl-2 and PCNA were inversely correlated with survival time [5,33].

Our results, concerning the differentiation of different tumour types, are promising and correct specimen classification rates of 70.3% for TC and WDNEC cases and 86.7% for WDNEC and SCLC cases could be achieved by means of chromatin texture and shape features. Comparable results have not yet been published.

By means of Cox regression analysis, subgroups of patients with different survival times can be separated using the chromatin patterns of the cell nuclei. In addition for each patient an individual survival curve can be evaluated and plotted according to an adaptive treatment scheme. This can be done even before surgery on the condition that a biopsy is available.

The largest drawback using high resolution image analysis in clinical routine is still the necessary amount of manual interaction for a clear segmentation of the nuclei. For each case about 45 minutes are needed for measuring and thresholding. However, there are several ongoing research projects in different laboratories to establish less time consuming (more automatic) segmentation methods.

Acknowledgment

We thank the team of the Munich Tumour Registry Center (Grosshadern, Germany) who made available the follow up data of the cancer patients.

Appendix. List of features and short description

Quantitative features are mostly derived from transformed extinction data in certain sub-regions of the nuclear region. They are identified by mnemos

BI..	Features from extinction data in the rim of the nuclear region
BICV	Coefficient of variation (CV) of density distribution of the rim
..	Features from extinction data of whole the nuclear region M1
	Mean of extinction distribution of whole nuclear region
M3	Skewness of extinction distribution of whole nuclear region
RFM1	Ratio of mean density of whole nucleus and rim (RFM1 = M1/BIM1)

D..	Dark particles derived from flat texture image. This is the difference image of a median filtered image with the original extinction image.
DM1	Mean extinction of dark particles
DM2	Standard deviation of extinction of dark particles
DNO	Number of dark particles
DCV	Coefficient of Variation of density distribution of dark particles (heterochromatin) (DCV = DM2/DM1)
DNOA	Relative number of dark particles (DNOA = DNO/A)
CO../NC..	Co-occurrence chromatin texture features derived from 2nd order statistics from pixels in the nuclear region from extinction (CO) and from flat texture (NC) [32])
CO9	Entropy
CO10	Difference variance
CO11	Difference entropy
CO14	Local mean
NC1	Co-occurrence 2nd order statistics of flat texture image: energy
RL../NR..	Run length parameters of texture from extinction (RL) and flat texture image (NR) [32]
RL1	Short runs emphasis
RL4	Run length non-uniformity
NR3	Gray level non-uniformity (flat texture image)
HU../HL..	Upper and lower half-height areas of nucleus consist of all connected dark and bright blob-like components of the nucleus. They are derived from a gray scale skeleton called *watershed*.
HUCV	Coefficient of variation
HUNO	Number of bright regions (particles)
HLNO	Number of dark regions (particles)
HUMIN	Minimum extinction
HUMAX	Maximum extinction
HUEULER	Connectivity number of upper and lower half-height areas (HUEULER = HUNO − HLNO), comparable with the Euler connectivity number as the number of holes minus the number of voids
HUSPAN	Range of upper half-height extinction (HUSPAN = HUMAX − HUMIN)
I../M..	Invariant moments of extinction weighted nucleus region (I..) and of the pure nucleus region. Invariant moments describe shapes. (Reference Fu)
IM2	2nd invariant moment
MM3	3rd invariant moment
..	Chromatin features after Mayall/Young [42]
CLUMP	Amount of chromatin clumping
HETERO	Heterogeneity of chromatin
..	Morphological features
A	Area (number of pixels) of nuclear region
P	Perimeter of nuclear region
FO1	Shape: Ratio of long and short diameter of nucleus

References

[1] M. Aubele, G. Burger and K. Rodenacker, Problems concerning the quality of DNA measurements on Feulgen-stained imprints. A study of five fixation techniques, *Analyt. Quant. Cytol. Histol.* **16**(3) (1994), 226–232.

[2] A. Böcking, C.P. Adler, H.H. Common, M. Hilgarth, B. Granzen and W. Auffermann, Algorithm for a DNA-cytophotometric diagnosis and grading of malignancy, *Analyt. Quant. Cytol.* **6** (1984), 1–7.

[3] A. Böcking, F. Giroud and A. Reith, Consensus report of the ESACP task force on standardization of diagnostic DNA image cytometry, *Analyt. Cell. Pathol.* **8** (1995), 67–74.

[4] J. Böhm, V. Kacic, P. Gais, H.W. Präuer and H. Höfler, Prognostic value of nucleolar organizer regions in neuroendocrine tumours of the lung, *Histochem.* **99** (1993), 85–90.

[5] J. Böhm, S. Koch, P. Gais, U. Jütting, H.W. Präuer and H. Höfler, Prognostic value of MIB-1 in neuroendocrine tumours of the lung, *Journal of Pathology* **178** (1996), 402–409.

[6] G. Burger and U. Jütting, Specimen classification in cytometry: an intercomparison of various means of decision making, in: E.S. Gelsema and L.N. Kanal, eds, *Pattern Recognition in Practice II*, North-Holland Publ., Amsterdam, 1985, pp. 509–519.

[7] C. Capella, P.U. Heitz, H. Höfler, E. Solcia and G. Klöppel, Revised classification of neuroendocrine tumours of the lung, pancreas and gut, *Virchows Arch.* **425** (1995), 547–560.

[8] F.A. Carey, D. Lamb and C.C. Bird, Intertumoral heterogeneity of DNA content in lung cancer, *J. Clin. Pathol.* **65** (1990), 2266–2269.

[9] N.Z. Carp, D.D. Ellison, P.P. Brophy, P. Watts, M.C. Chang and S.M. Keller, DNA content in correlation with postsurgical stage in non-small cell lung cancer, *Ann. Thorac. Surg.* **53** (1992), 680–683.

[10] D.G. Davila, W.F. Dunn, H.D. Tazelaar and P.C. Pairolero, Bronchial carcinoid tumors, *Mayo Clin. Proc.* **68** (1993), 795–803.

[11] L. Desinan, C.A. Scott, S. Pizzolitto, C. Avellini, G. Rimondi, P. Bardus, V. Rizzi, G. Talmassons, C. Puricelli and C.A. Beltrami, Non-small cell lung cancer. Morphology and DNA flow cytometry, *Analyt. Quant. Cytol. Histol.* **18**(6) (1996), 438–452.

[12] P. Gais and G. Burger, Geräte zur quantitativen Mikroskopie, in: *Morphometrie in der Zyto- und Histopathologie*, G. Burger, M. Oberholzer and W. Gössner, eds, Springer Verlag, New York, 1988, pp. 282–294.

[13] F. Gao, U. Jütting, K. Rodenacker, P. Gais and P.Z. Lin, Relevance of chromatin features in the progression of esophageal epithelial severe dysplasia, *Analyt. Cell. Pathol.* **13** (1997), 17–28.

[14] F. Giroud, G. Haroske, A. Reith and A. Böcking, Proposal for the updated ESACP consensus report on diagnostic DNA image cytometry. (Not yet published, 1997.)

[15] V.E. Gould, R.I. Linnoila, V.A. Memoli and W.H. Warren, Neuroendocrine cells and neuroendocrine neoplasms of the lung, *Pathol. Annu.* **18** (1983), 287–330.

[16] A. Gschwendtner and T. Mairinger, How thick is your section? The influence of section thickness on DNA-cytometry on histological sections, *Analyt. Cell. Pathol.* **9** (1995), 29–37.

[17] G. Haroske, K.D. Kunze, V. Dimmer, W. Meyer and F. Theissig, Feasibility and limitations of cytometric DNA ploidy analysis procedures in tissue sections, *Zentbl. Pathol.* **139** (1994), 407–417.

[18] G. Haroske, W.D. Meyer, F. Theissig and K.D. Kunze, Increase of precision and accuracy of DNA cytometry by correcting diffraction and glare errors, *Analyt. Cell. Pathol.* **9** (1995), 1–12.

[19] H. Höfler, Spektrum neuroendokriner Tumoren der Lunge, *Pathologe* **18** (1997), 322–323.

[20] N. Ikeda, C. MacAulay, S. Lam, D. Garner, P. Payne, H. Kato, C. Konaka and B. Palcic, Use of high-resolution cytometry in predicting the biologic behavior of T1 adenocarcinoma of the lung, *Analyt. Quant. Cytol. Histol.* **17**(1) (1995), 69–74.

[21] E.L. Kaplan and P. Meier, Non-parametric estimation from incomplete observations, *J. Am. Stat. Assoc.* **53** (1958), 457–481.

[22] T. Kawai, M. Suzuki, S. Kono, N. Shinomiya, M. Rokutanda, K. Takagi, T. Ogata and S. Tamai, Proliferating cell nuclear antigen and Ki-67 in lung carcinoma. Correlation with DNA flow cytometric analysis, *Cancer* **74**(9) (1994), 2468–2475.

[23] J.A. Kern and A.E. Filderman, Oncogenes and growth factors in human lung cancer, *Clin. Chest. Med.* **14**(1) (1993), 31–41.

[24] S. Lam, C. MacAulay and B. Palcic, Detection and localization of early lung cancer by image techniques, *Chest* **103** (1993), 12S–14S.

[25] E.T. Lee, *Statistical Methods for Survival Data Analysis*, Lifetime Learning Publications, Belmont, CA, 1980, pp. 298–337.

[26] C. MacAulay and B. Palcic, Fractal texture features based on optical density surface area: use in image analysis of cervical cells, *Analyt. Quant. Cytol. Histol.* **12** (1990), 394–398.

[27] P.A. McCue and G.C. Finkel, Small-cell carcinoma: an evolving histopathological spectrum, *Semin. Oncol.* **20** (1993), 153–162.

[28] C.F. Mountain, A new international staging system for lung cancer, *Chest* **89** (1986), 225s–233s.

[29] J.C. Pence, B.J. Kerns, R.K. Dodge and J.D. Iglehart, Prognostic significance of the proliferation index in surgically resected non-small-cell lung cancer, *Arch. Surg.* **128**(12) (1993), 1382–1390.

[30] J.L. Pujol, J. Simony, G. Jolimoy, D. Jaffuel, P. Demoly, X. Quantin, C. Marty-Ane, J.M. Boher, R. Charpentier and F.B. Michel, Hypodiploidy, Ki-67 growth fraction and prognosis of surgically resected lung cancers, *Br. J. Cancer* **74**(6) (1996), 964–970.

[31] K. Rodenacker, Featuring of cellular objects, in: *Clinical Cytometry and Histometry*, G. Burger, J.S. Ploem and K. Goerttler, eds. Rep. Part 3.4, 1973, pp. 73–78.

[32] K. Rodenacker, Invariance of textural features in image cytometry under variation of size and pixel magnitude, *Analyt. Cell. Pathol.* **8** (1995), 117–133.

[33] G.V. Scagliotti, M. Micela, L. Gubetta, E. Leonardo, S. Cappia, P. Borasio and E. Pozzi, Prognostic significance of KI-67 labelling in resected non small cell lung cancer, *Eur. J. Cancer.* **29A**(3) (1993), 363–365.

[34] A. Schalhorn ed., *Empfehlungen zur Diagnostik, Therapie und Nachsorge: Tumoren der Lunge und des Mediastinums*, Tumorzentrum München, 1997. http://www.med.uni-muenchen.de/tzm/empfehlung/bc4/homepage.html

[35] U. Schenck, U. Jütting and K. Rodenacker, Modelling, definition and applications of histogram features based on DNA values weighed by SINE functions, *Analyt. Quant. Cytol. Histol.* **19** (1997), 443–452.

[36] B. Stenkvist and G. Strande, Entropy as an algorithm for the statistical description of DNA cytometric data obtained by image analysis microscopy, *Analyt. Cell. Path.* **2** (1990), 159–165.

[37] D. Tirindelli-Danesi, L. Teodori, F. Mauro, C. Modini, C. Botti, F. Cicconetti and S. Stipa, Prognostic significance of flow cytometry in lung cancer: a 5-year study, *Cancer* **60** (1987), 844–851.

[38] W.H. Warren, L.P. Faber and V.E. Gould, Neuroendocrine neoplasms of the lung. A clinicopathologic update, *J. Thorax Cardiovasc. Surg.* **98** (1989), 321–332.

[39] W.H. Warren and V.E. Gould, Neuroendocrine neoplasms of the lung. A 10 year perspective of their classification, *Zentralbl. Pathol.* **139** (1993), 107–113.

[40] G. Wolf, M. Bell and H. Guski, Chromatin structure analysis based on a hierarchic texture model, *Analyt. Quant. Cytol. Histol.* **17** (1995), 25–34.

[41] World Health Organization, The W.H.O. histologic typing of lung tumours. 2nd ed., *Am. J. Clin. Pathol.* **77** (1998), 123–136.

[42] I.T. Young, P.W. Verbeek and B.H. Mayall, Characterization of chromatin distribution in cell nuclei, *Cytometry* **7** (1986), 467–474.